Supporting information for: The role of through-space interactions in modulating constructive and destructive interference effects in benzene

Anders Borges,[†,‡] Jianlong Xia,[¶] Sheng Hua Liu,[§] Latha Venkataraman,[*,‖] and Gemma C. Solomon[*,‡]

†*Department of Applied Physics, Columbia University, New York*

‡*Nano-Science Center and Department of Chemistry, University of Copenhagen, Copenhagen*

¶*School of Chemistry, Chemical Engineering and Life Science, Wuhan University of Technology, Wuhan 430070, China*

§*Key Laboratory of Pesticide and Chemical Biology, Ministry of Education, College of Chemistry, Central China Normal University, Wuhan, 430079, China*

‖*Department of Applied Physics and Department of Chemistry, Columbia University, New York*

E-mail: lv2117@columbia.edu; gsolomon@nano.ku.dk

Contents

1 Derivation of analytical results

We derive here the analytical lineshapes shown in Figure 3. We assume a non-interacting tight binding model in an orthogonal basis with six basis functions, each centered on a C in benzene and coupled to nearest neighbors through hopping terms $-t$ in the Hamiltonian. The onsite energy of each site is set to 0. The Hamiltonian of this system can be written in matrix form as

$$\mathbf{H} = \begin{bmatrix} 0 & -t & 0 & 0 & 0 & -t \\ -t & 0 & -t & 0 & 0 & 0 \\ 0 & -t & 0 & -t & 0 & 0 \\ 0 & 0 & -t & 0 & -t & 0 \\ 0 & 0 & 0 & -t & 0 & -t \\ -t & 0 & 0 & 0 & -t & 0 \end{bmatrix} \tag{1}$$

We model the left lead as an infinite one-dimensional metallic chain with onsite-elements set to zero and nearest neighbor hopping terms set to -p. The first site in the chain is the only site that is electronically coupled to the molecule. A sketch of the model is shown in Figure S1.

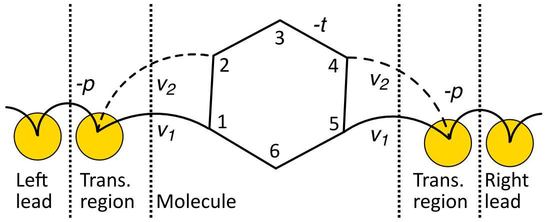

Figure S1: Model system used to calculate analytical results.

We use the method of transition regions as outlined by Thygesen and Rubio[S1] and regard the first site in the chain as the transition region. It can be shown that the self energy of the molecule in the presence of the left leads is then $\mathbf{\Sigma}_L(E) = \mathbf{h}_{MT} g^r_T(E)\mathbf{h}_{TM}$, where g^r_T is the retarded Green's function of the last site in the chain in the presence of the rest of the chain calculated as $(E - \Sigma_T)^{-1}$. $\mathbf{h}_{MT}$ is the submatrix describing hopping elements in the Hamiltonian between the transition region and the molecule and Σ_T is the left lead self energy onto last site of the chain. If we assume that only the 1st and 2nd site in the molecule couples to the leads with coupling strengths v_1 and v_2 respectively we can find the submatrix of the left self energy corresponding to site 1 and 2 in the presence of the chain as

$$\begin{bmatrix} v_1^2 & v_1v_2 \\ v_1v_2 & v_2^2 \end{bmatrix} g_T^r \tag{2}$$

In the wide-band limit, this matrix is purely imaginary and energy-independent. Defining $v_1^2 g_T^R = i\gamma$ and $x = v_2/v_1$ as the relative conductance we can write the submatrix as

$$\begin{bmatrix} 1 & x \\ x & x^2 \end{bmatrix} i\gamma \tag{3}$$

The same can be done for the right lead.

The zero-bias conductance is calcutated as $dI/dV|_{V=0} = G_0T(E_F)$ where the transmission is calculated using the Landauer formula:

$$T(E_F) = \sum_{ijkl} \Gamma_{ij}^L(E_F)G_{jk}^r(E_F)\Gamma_{kl}^R(E_F)G_{ki}^a(E_F) \tag{4}$$

Here Γ_{ij}^L is the i, j'th element of the energy dependent left broadening matrix defined as $\mathbf{\Gamma}^L = -2Im(\mathbf{\Sigma}_L)$ and we therefore find:

$$\mathbf{\Gamma}^L = -2\gamma \begin{bmatrix} 1 & x & 0 & 0 & 0 & 0 \\ x & x^2 & 0 & 0 & 0 & 0 \\ 0 & 0 & 0 & 0 & 0 & 0 \\ 0 & 0 & 0 & 0 & 0 & 0 \\ 0 & 0 & 0 & 0 & 0 & 0 \\ 0 & 0 & 0 & 0 & 0 & 0 \end{bmatrix} \tag{5}$$

Given this matrix, we can evaluate x as $\sqrt{\Gamma_{22}^L/\Gamma_{11}^L}$ or $\Gamma_{21}^L/\Gamma_{11}^L$. In order to calculate the zero-bias conductance we also need the retarded Green's function of the molecule at the Fermi energy which is defined as our zero-point in energy. This is calculated as $\mathbf{G}^r(E_F) = [-\mathbf{H} - \mathbf{\Sigma}_L - \mathbf{\Sigma}_R]^{-1}$. In the limit of weak coupling and far from molecular resonances this can be approximated as $\mathbf{G}^r(E_F) = [-\mathbf{H}]^{-1}$. The matrix elements of this Green's function can be calculated analytically. Using Cramer's formula it is easily shown that the Green's function elements between sites that are meta- to each other vanish and sites that are ortho or para- to each other equal $\frac{1}{2t}$ and $-\frac{1}{2t}$ respectively. We are now in a position to evaluate the conductance in the four regimes proposed in the paper.

1.1 *meta-2*

In regime I we have

$$\Gamma^L_{11} = \Gamma^R_{55} = -2\gamma \tag{6}$$

for the sites coupled the strongest to the electrodes. The off-diagonal elements are

$$\Gamma^L_{12} = \Gamma^L_{21} = \Gamma^R_{65} = \Gamma^R_{56} = -2\gamma x \tag{7}$$

The remaining non-zero elements are

$$\Gamma^L_{22} = \Gamma^R_{66} = -2\gamma x^2. \tag{8}$$

We can therefore calculate the transmission at the Fermi energy as

$$T(E_F) = \Gamma^L_{11} G^r_{61} \Gamma^R_{16} G^a_{61} + \Gamma^L_{22} G^r_{25} \Gamma^R_{55} G^a_{52} + \Gamma^L_{12} G^r_{25} \Gamma^R_{56} G^R_{61} + \Gamma^L_{21} G^r_{16} \Gamma^R_{65} G^{52} = 0 \tag{9}$$

Here the first two terms cancel with the last two due to the opposite signs of G^r_{25} and G^r_{16} and robust destructive interference is observed. This cancellation is not present in the classical (incoherent) case where off-diagonal elements in Γ are zero.

1.2 *meta-1*

For *meta-1* we have

$$\Gamma^L_{11} = \Gamma^R_{55} = -2\gamma \tag{10}$$

and the off-diagonal terms are

$$\Gamma^L_{12} = \Gamma^L_{21} = \Gamma^R_{45} = \Gamma^R_{54} = -2\gamma x. \tag{11}$$

The remaining non-zero elements are

$$\Gamma^L_{22} = \Gamma^R_{44} = -2\gamma x^2. \tag{12}$$

Hence, the transmission at the Fermi energy is

$$T(E_F) = \Gamma^L_{11} G^r_{14} \Gamma^R_{44} G^a_{41} + \Gamma^L_{21} G^r_{14} \Gamma^R_{45} G^a_{52} + \Gamma^L_{12} G^r_{25} \Gamma^R_{54} G^R_{41} + \Gamma^L_{22} G^r_{25} \Gamma^R_{55} G^{52} = 4x^4 T_0, \tag{13}$$

where $T_0 = \gamma^2/t^2$ is the conductance of a single para-coupled molecule. Here the through-space interaction leads to a constructive contribution.

1.3 *para-1*

In this regime we find similarly:

$$\Gamma^L_{11} = \Gamma^R_{44} = -2\gamma \tag{14}$$

and

$$\Gamma^L_{12} = \Gamma^L_{21} = \Gamma^R_{45} = \Gamma^R_{54} = -2\gamma x \tag{15}$$

$$\Gamma^L_{22} = \Gamma^R_{55} = -2\gamma x^2. \tag{16}$$

We then have

$$T(E_F) = \Gamma^L_{11} G^r_{14} \Gamma^R_{44} G^a_{41} + \Gamma^L_{22} G^r_{25} \Gamma^R_{55} G^a_{52} + \Gamma^L_{12} G^r_{25} \Gamma^R_{54} G^R_{41} + \Gamma^L_{21} G^r_{14} \Gamma^R_{44} G^{42} = (1 + 2x^2 + x^4) T_0 \tag{17}$$

In this regime we again see constructive interference.

1.4 *para-2*

In the final regime, we have:

$$\Gamma^L_{22} = \Gamma^R_{55} = -2\gamma \tag{18}$$

$$\Gamma^L_{12} = \Gamma^L_{21} = \Gamma^R_{56} = \Gamma^R_{65} = -2\gamma x \tag{19}$$

$$\Gamma^L_{11} = \Gamma^R_{66} = -2\gamma x^2 \tag{20}$$

Finally we find

$$G = \Gamma^L_{11} G^r_{16} \Gamma^R_{66} G^a_{61} + \Gamma^L_{22} G^r_{25} \Gamma^R_{55} G^a_{52} + \Gamma^L_{12} G^r_{25} \Gamma^R_{56} G^R_{61} + \Gamma^L_{21} G^r_{16} \Gamma^R_{65} G^{52} = (1 - 2x^2 + x^4) T_0. \tag{21}$$

Here the last two terms have the opposite sign as the first two and we therefore see destructive interference. This destructive interference is not present in the incoherent case where off-diagonal elements of $\mathbf{\Gamma}^{L/R}$ are zero. The conductance as function of relative coupling can then be plotted along the axes as has been done in Figure 4. The analytical results rely on the approximation that $\mathbf{G}^r(E_F) = [-\mathbf{H}]^{-1}$, i.e. the the lead self energies can be ignored. Figure S2 allows us to evaluate the validity of the approximation. The full line shows the calculated line-shapes in the weak coupling limit where the largest element of $\mathbf{\Gamma}^{L/R}$ is 0.001 eV. This limit corresponds to our analytical result. The dashed line shows the calculated line-shape where the largest element of $\mathbf{\Gamma}^{L/R}$ is 1.0 eV. The close resemblance of the two curves show that the approximation is accurate even for stronger coupling to the leads.

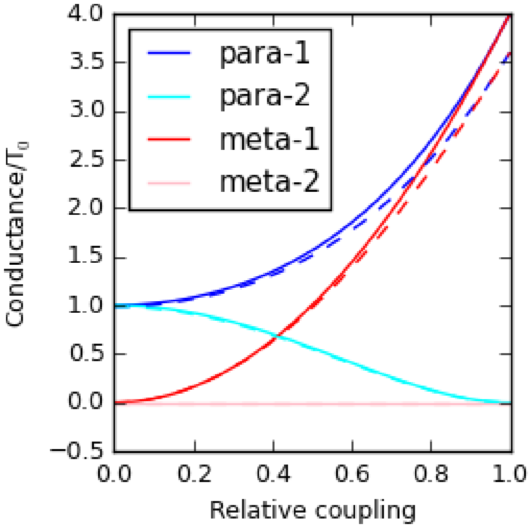

Figure S2: Dependence of line-shapes on the strength of the coupling for $t = -2.8$ eV. Full line: Largest element of $\mathbf{\Gamma}^{L/R}$ is 0.001 eV. Dashed line: Largest element of $\mathbf{\Gamma}^{L/R}$ is 1 eV.

2 Superposition law of benzene molecules in parallel

We derive here the sources of imperfect constructive interference in parallel molecular wires. We assume a tight binding model where the last site of a metallic chain couples to a molecule from both sides. Assume that only the sites labelled a and b coupled to the left and right site respectively. In this case the transmission is equal to

$$T(E) = \Gamma_{aa} G^r_{ab} \Gamma_{bb} G^a_{ba} \tag{22}$$

where $G^r_{ab} = [E\mathbf{S} - \mathbf{H} - \mathbf{\Sigma}]^{-1}_{ab} = [\mathbf{A}]^{-1}_{ab}$. Suppose we couple a second molecule in parallel via the same site in the chain with equal strength such that A is of the form $\mathbf{A} = \mathbf{A}_1 + \mathbf{A}_2 + \mathbf{A}_{12}$ where $\mathbf{A}_1(\mathbf{A}_2)$ only has elements corresponding to sites on the first(second) molecule and $\mathbf{A}_{12}$ only contains off-diagonal elements between sites belonging to the two molecules. We denote the sites coupling to the left and right chain as sites A and B and assume they couple equally strong as a and b. Then we know that $\Gamma^L_{aa} = \Gamma^L_{AA} = \Gamma^L_{Aa} = \Gamma^L_{aA} = -2\gamma$. We then find that the total transmission is equal to

$$T(E) = \Gamma^L_{aa} G^r_{ab} \Gamma^R_{bb} G^a_{ba} + \Gamma^L_{AA} G^r_{AB} \Gamma^R_{BB} G^a_{BA} + \Gamma^L_{Aa} G^r_{ab} \Gamma^R_{bB} G^a_{BA} + \Gamma^L_{aA} G^r_{AB} \Gamma^R_{Bb} G^a_{ba}. \tag{23}$$

Suppose A is block-diagonal with respect to each ring. This occurs in the limit of weak coupling to the leads and between the wires. In this case

$$G^r_{ab} \approx [\mathbf{A}_1]^{-1}_{ab} \tag{24}$$

and G^r_{ab} therefore does not depend on the second molecule. When both molecules are identical, each term in equation 23 evaluates to the same value and the total transmission is therefore equal to four times the transmission of the individual molecule. In the case where each molecule is coupled to separate sets of leads the off-diagonal terms in the Γ^L and Γ^R vanish and we recover the classical result.

3 Evaluation of the conductance ratios

In order to estimate the conductance ratios G_{DD}/G_{SD} and $G_{DD,cut}/G_{SD}$ we start by obtaining the Hamiltonian and overlap matrix of the scattering region. We then divide the basis functions centered on the individual atoms into different sets as shown in Figure S3. Basis functions centered on atoms outside an indicated box are taken to belong the left or right electrode as appropriate. To calculate the conductance of a single half of the molecule we cut all off diagonal elements coupling basis functions on different rings and calculate $G^r_{cut} = [\mathbf{A}_1 + \mathbf{A}_2]^{-1}$. We then calculate G_{SD} as

$$G_{SD} = \frac{1}{2} G_0 \left(\sum_{ijkl \in \text{Ring 1}} \Gamma^L_{ij} G^r_{cut,jk} \Gamma^R_{kl} G^a_{cut,ki} + \sum_{ijkl \in \text{Ring 2}} \Gamma^L_{ij} G^r_{cut,jk} \Gamma^R_{kl} G^a_{cut,ki} \right) \tag{25}$$

where all matrices are evaluated at the Fermi energy. We then calculate $G_{DD,cut}$ as:

$$G_{DD,cut} = G_0 \sum_{ijkl} \Gamma^L_{ij} G^r_{cut,jk} \Gamma^R_{kl} G^a_{cut,ki} \tag{26}$$

This means that we retain off-diagonal elements in Γ^L and Γ^R. In the case of perfect coherence the ratio $G_{DD,cut}/G_{SS}$ should tend towards four.

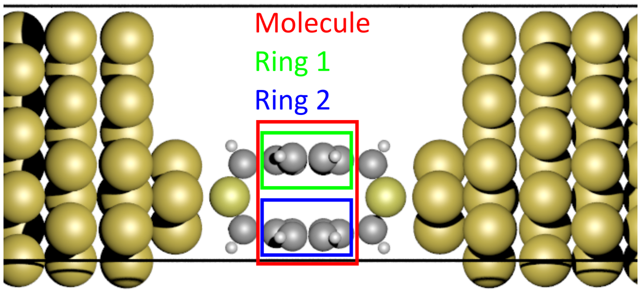

Figure S3: Specification of regions used to calculate conductance ratio.

4 Computational details

We used ASE/GPAW for the electronic structure calculations and the PBE functional for all calculations. To obtain junction geometries we constructed a 4x4x4 Au(111) slab with either a trimer or a four atom pyramid on both sides of the slab and used periodic binding geometries to simulate a junction. A molecule was placed in the junction and the innermost two layers of Au in the slab was held at the bulk positions while the remaining atoms were relaxed to within a maximum force of 0.04 eV/A using a 2x2 Monchhorst-Pack k-point sampling. The length of the cell was then extended/reduced in increments of 0.2 Å and relaxed after each step to simulate extension/pushing of the junction. This procedure was repeated until a potential energy surface around a local minima had been established. For the transport calculations we added six more layers of Au to the bulk part of the relaxed junction and obtained the Hamiltonian and overlap matrix for the junction as input to the

ASE transport calculator using a Monchhorst-Pack k-point sampling of 4x4. The transport calculator also requires the overlap and electronic couplings between principal layers in the Au. To evaluate this we ran a DFT calculation on nine layers of Au using the same setting as for the full junction. We used three Au layers per principal layer. The lead self energies were evaluated using the ASE transport calculator and the size of the central region was changed using the method of transition regions outlined in the previous sections.

5 Symmetry partitioning and six site model

We used the same symmetry partitioning as outlined in detail previously[S2,S3] with a few exceptions. The flexible linker groups in **1** and **2** makes it difficult to obtain the exact same basis set for all junction geometries. For every relaxed junction geometry we therefore cut out the benzene ring from the center of the molecule and replaced the linker groups with hydrogens and placed it in a cell with the same orientation as in the junction. We then relaxed the geometry of the benzene molecule under the constraint that the two C's bound to the linker groups were fixed in space. We then ran a self-consistent DFT calculation on the molecule to obtain the Hamiltonian and overlap matrix from which we partitioned the basis set into σ and π by subdiagonalizing the Hamiltonian corresponding to each atom. We then rotated the junction Hamiltonian corresponding to the benzene molecule into the linear combination of atom-centered basis functions that subdiagonalized the gas phase Hamiltonian corresponding to each atom. This ensured that an identical symmetry-partitioning was used for all junction geometries. By defining the central region as that of all basis functions centered on the benzene ring (linker groups and Au belonging to left and right electrode as appropriate) all basis functions in the central region could be assigned either σ or π symmetry. This allowed us to partition the transmission into σ, π and σ/π contributions as:

$$T(E) = \sum_{ijkl} \Gamma^L_{ij} G^r_{jk} \Gamma^R_{kl} G^a_{li} = T_\sigma + T_\pi + T_{\sigma/\pi} \tag{27}$$

Here, T_σ is the sum of all terms where i, j, k, l belong to the σ set. T_π is defined in the same way. $T_{\sigma/\pi}$ are the remaining terms in the sum.

The relaxation of the benzene molecule in vacuum also meant that we could find the linear combination of basis function in the junction that made up the p_z orbitals in vacuum. As p_z orbitals we used the partially occupied maximally localized Wannier functions as described by Thygesen et al[S4] and implemented in ASE. We replaced the basis set of the benzene core of the molecules in the junction with the six linear combinations that represented the p_z orbitals of benzene in the gas phase. Tiny geometry distortions arising from the relaxation in the gas phase and missing contributions from removed basis functions centered on H meant the overlap matrix of the p_z orbitals in the junction was not perfectly orthogonal as is assumed in the analytical model. Still, we believe that our method is the best possible way to obtain parameters for the six site model from a full DFT calculation.

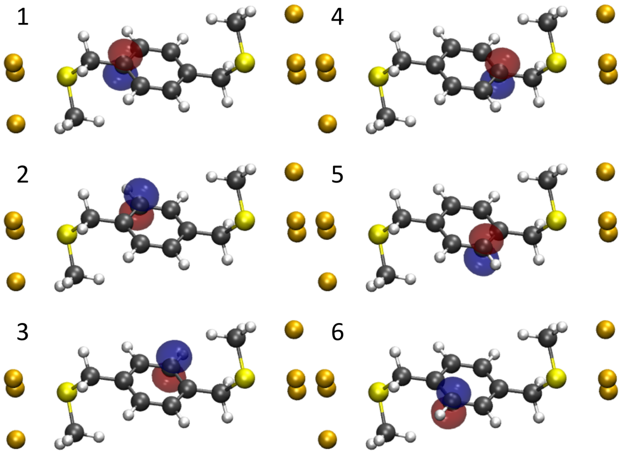

Figure S4: Sample basis used to extract six site model. Numbers indicate basis label.

As an example we show in Figure S4 the extracted six site basis for a sample geometry of **1**. In Equation 28 we show the extracted effective Hamiltonian for the sample.

$$\mathbf{H}+Re(\mathbf{\Sigma}_L(E_F))+Re(\mathbf{\Sigma}_R(E_F))=\begin{bmatrix} -0.12 & 2.81 & -0.19 & -0.23 & 0.20 & 2.92 \\ 2.81 & -0.24 & -2.85 & -0.20 & 0.27 & -0.06 \\ -0.19 & -2.85 & -0.33 & 2.92 & 0.05 & -0.27 \\ -0.23 & -0.2 & 2.92 & -0.10 & -2.81 & -0.20 \\ 0.20 & 0.27 & 0.05 & -2.81 & -0.24 & 2.85 \\ 2.92 & -0.06 & -0.27 & -0.20 & 2.85 & -0.33 \end{bmatrix} \tag{28}$$

Below we show the equivalent left broadening matrix:

$$\mathbf{\Gamma}^L(E_F)=\begin{bmatrix} 0.22 & -0.10 & -0.01 & -0.00 & -0.00 & -0.03 \\ -0.10 & 0.05 & 0.00 & 0.00 & 0.00 & 0.01 \\ -0.01 & 0.00 & 0.00 & 0.00 & 0.00 & 0.00 \\ -0.00 & 0.00 & 0.00 & 0.00 & 0.00 & 0.00 \\ -0.00 & 0.00 & 0.00 & 0.00 & 0.00 & -0.00 \\ -0.03 & 0.01 & 0.00 & 0.00 & -0.00 & 0.01 \end{bmatrix} \tag{29}$$

This shows that the basis functions with index 1 and 2 couple strongest to the left leads. It also shows that the assumption in the model that only two sites couple to the each lead is an approximation. From $\mathbf{\Gamma}_L$ we can evaluate the relative coupling in the two ways:

$$x=\sqrt{\Gamma^L_{22}/\Gamma^L_{11}}=0.46 \tag{30}$$

or

$$x=\Gamma^L_{21}/\Gamma^L_{11}=0.45. \tag{31}$$

In determining x for each junction we use both ways on both $\mathbf{\Gamma}^L$ and $\mathbf{\Gamma}^R$ and take the average. The resulting values of x are shown in Figure S5. Here we see that realistic values of x range from 0.2 to 0.6 as a result of the flexible nature of the linker.

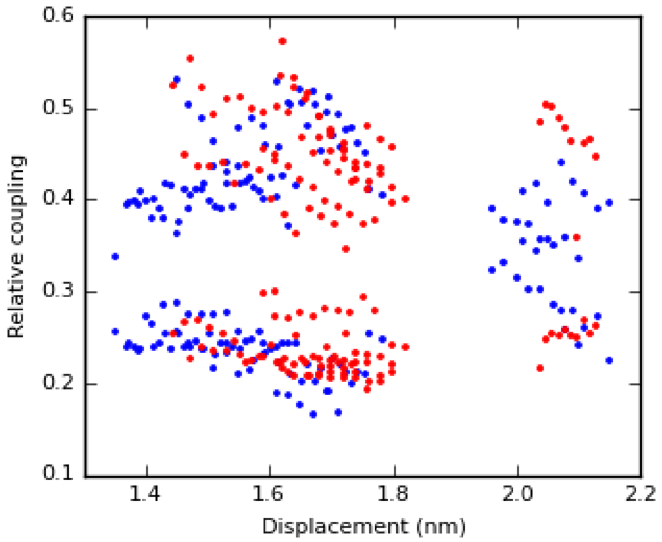

Figure S5: Average value of relative coupling (x) for 168 junction geometries of **1**(red dots) and **2** (blue dots).

6 Validity of symmetry partitioning and six site model

As outlined in the introduction it has been difficult to observe destructive interference for short molecules. We therefore probe the conductance as the junction is extended for the molecules shown in Figure 1(a). Our rotation of molecular basis functions allows us to evaluate the contribution to the transmission from both σ, π, and σ/π. To convince the reader that the partitioning is sensible we plot first the partitioned transmission of two junctions in Figure S6. Figure S6(a) shows the partitioned transmission of a para-substituted molecule which is not expected to show destructive interference. The black line shows the full calculated transmission. The magenta line shows the transmission through the σ system while the cyan line shows the transmission through the π system. The gray line show the mixed σ/π term. It is seen that the transport throughout the band gap of the molecule is dominated by the π system with contribution to transport from the σ system being orders of magnitude lower. Also shown in the figure is the transport through the model π system obtained consisting of the six p_z orbitals. We see that the transmission is almost identical to the full transmission. This clearly indicates that the six site model works very well for this particular junction geometry. It works less well for the meta-coupled molecule shown in Figure S6(b). The full transmission is lower in the band gap for this molecule but the characteristic antiresonance in the band gap is not apparent. We also see that the σ contribution at the Fermi energy is an order or magnitude higher than for the para-coupled molecule. Even so, the total transmission is dominated by the π system which is equally well represented by the π contribution to the transport as the six site model system labeled Wannier π.

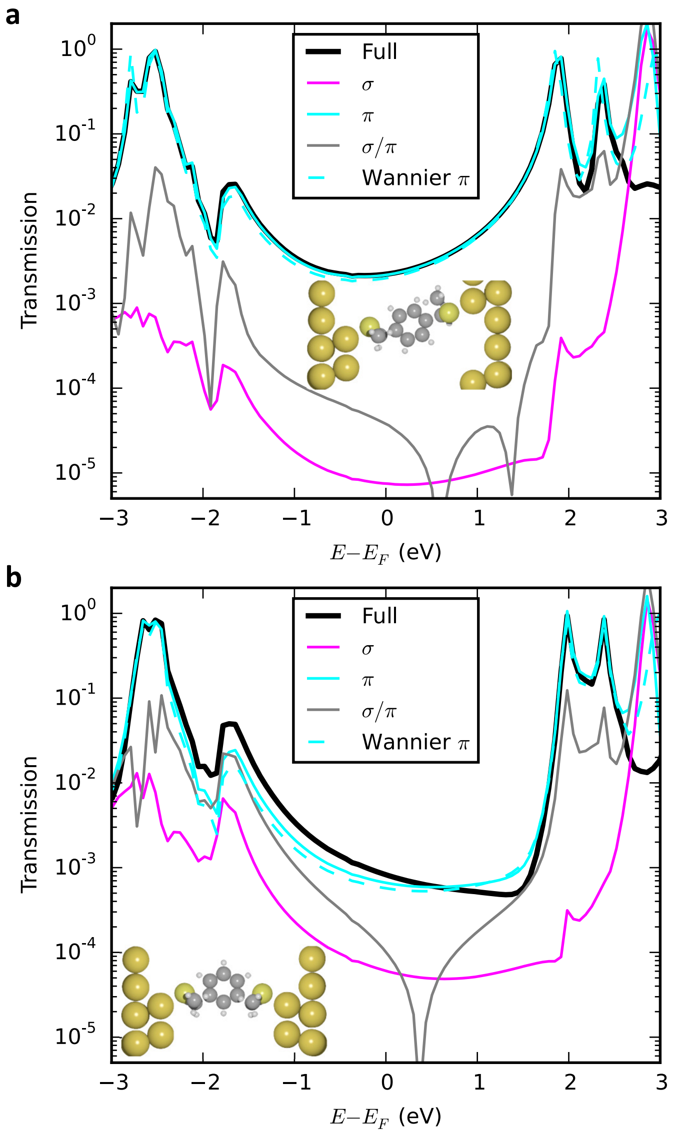

Figure S6: Partitioned transmission. Insert shows geometry. a) Partitioned transmission of **1**. b) Partitioned transmission of **2**.

These single junction geometry do not necessarily represent the full width of experimentally probed junction geometries. We therefore repeated the calculations for the 168 individual junction geometries containing **1** or **2**. Figure S7 shows the partitioned transmission at the Fermi energy for six different binding geometries and molecular conformations around local minima on the potential energy surface. The black dots represent the total conductance and the magenta/cyan and gray dots represent the σ/π and mixed σ/π contributions. The blue dots represent the conductance calculated through the six site model. This shows that the σ contribution consistently does not contribute to the conductance and that the π system is the major contributor to the conductance. It also shows that the six site model reproduces the same conductance as the π system. This indicates that the six site model can represent the full calculation. Taking the average of all dots in the six panels gives the numbers shown in Table 1. Figure S8 shows the equivalent plot for **2**. Again, we see that the partitioning in most cases is reasonable.

7 Gateway state for 4

The calculated transport properties corresponding to *meta-2* of **4** was distinctly different from our calculations on *meta-1*, *para-1* and *para-2* because the zero-bias conductance could not be partitioned into symmetry components as discussed in the paper. We associated this with the occurrence of a gateway state. Such a gateway state would imply a strong dependence of the conductance upon breaking of the Au-S bond. We therefore plotted the conductance as function of displacement for fully relaxed junctions of *meta-1* and *meta-2*. The result is shown in Figure S9(a). This shows a strong dependence of conductance on displacement for *meta-2* but no for *meta-1*. Figure S9(b) shows the calculated transmission at the displacement corresponding to the lowest energy in (a). Figure S9(c) shows the density difference upon binding of the molecule to Au at the lowest energy displacement in (a). The change in density is clearly largest around the bonds between S and Au indicating a change

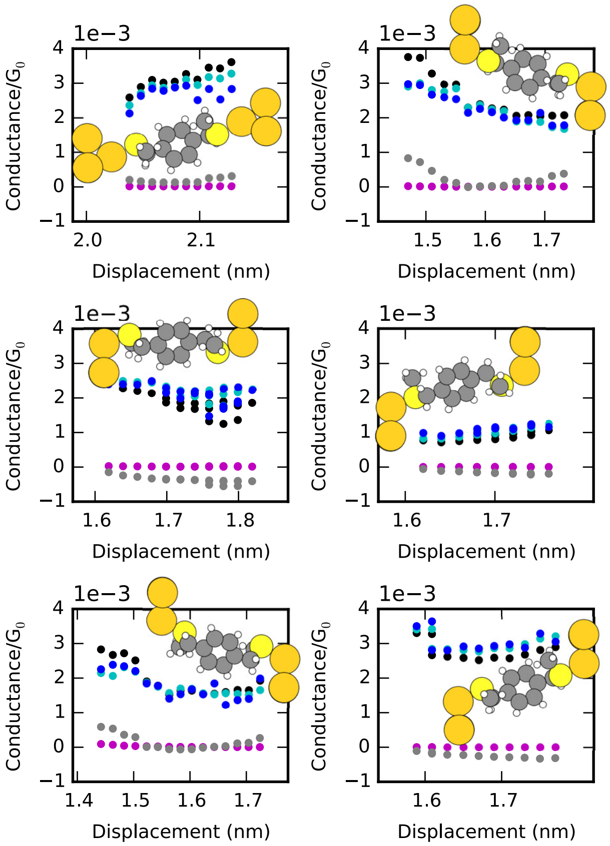

Figure S7: Partitioned zero-bias conductance for **1**. Black dots: Full conductance. Blue dots: π contribution. Magenta dots: σ contribution. Gray dots: σ/π contribution. Cyan dots: Calculated conductance from extracted six site model.

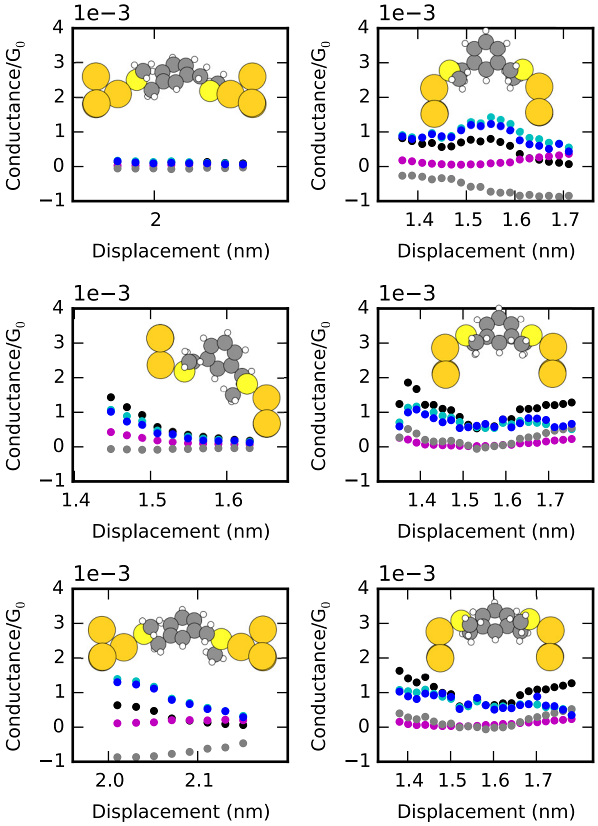

Figure S8: Partitioned zero-bias conductance for **2**.Black dots: Full conductance. Blue dots: π contribution. Magenta dots: σ contribution. Gray dots: σ/π contribution. Cyan dots: Calculated conductance from extracted six site model.

in the electronic structure upon binding in this particular region. Notice how the left "bond" on *meta-2* points more in the direction of the second bond than for *meta-1*. Combined with the shorter distance, we believe this is the reason why the conductance of only this isomer is dominated by the gateway state.

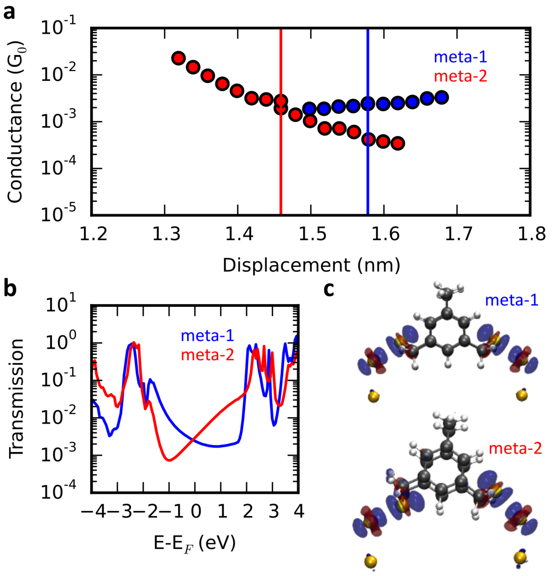

Figure S9: a) Conductance as function of displacement for *meta-1* and *meta-2* for **4**. Vertical lines indicate displacement corresponding to a minimum on the potential energy surface. b) Calculated transmission at displacements corresponding to vertical lines in (a). c) Density difference upon binding.

8 Synthesis of 2

2

Figure S10: Synthetis of **2**

To a degassed solution of 0.61 g (3.6 mmol) of 1,3-phenylenedimethanethiol[S5] in DMF (20 mL) was added 0.5 mL (8 mmol) of iodomethane under nitrogen, K2CO3 (1.0g 7.2 mmol) was added and the reaction mixture was stirred for 24h at room temperature. The reaction was quenched with 50 mL of water and cooled at 4° C overnight. The resulting suspension was filtered and washed with water. The crude product was purified by chromatography on silica and eluted with CHCl3/hexane (1:4) to give compound 2 as a white solid (286 mg, 40%). ^{1}H NMR (400 MHz, CDCl3) shown in Figure S11: 1.99 (s, 6H, CH3), 3.66 (s, 4H, CH2), 7.17-7.27 (m, 4H, Ar-H). ^{13}C NMR (150 MHz, CDCl3) shown in Figure S12: 14.55 (CH3), 37.79 (CH2), 127.12, 128.17, 128.94, 138.07(Ar). Anal. Calcd for C10H14S2: C, 60.55; H, 7.11. Found: C, 60.68; H, 7.40.

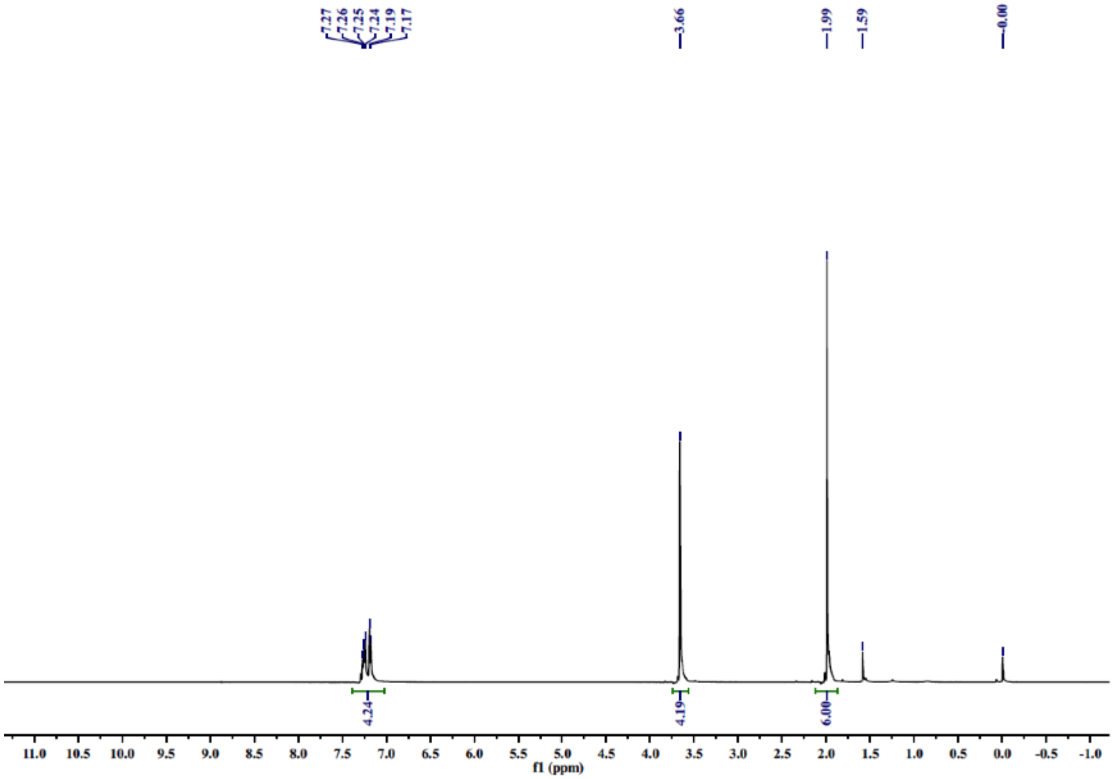

Figure S11: ^{1}H NMR spectrum of compound **2**.

9 Conformers of 4

For **3**, the binding groups force the two benzene rings to be held in a "sandwich"-like geometry where the two benzene rings are coplanar. As a result, only two conformers are possible and these are shown in Table 2 in the main paper. **4** can however exist in several different

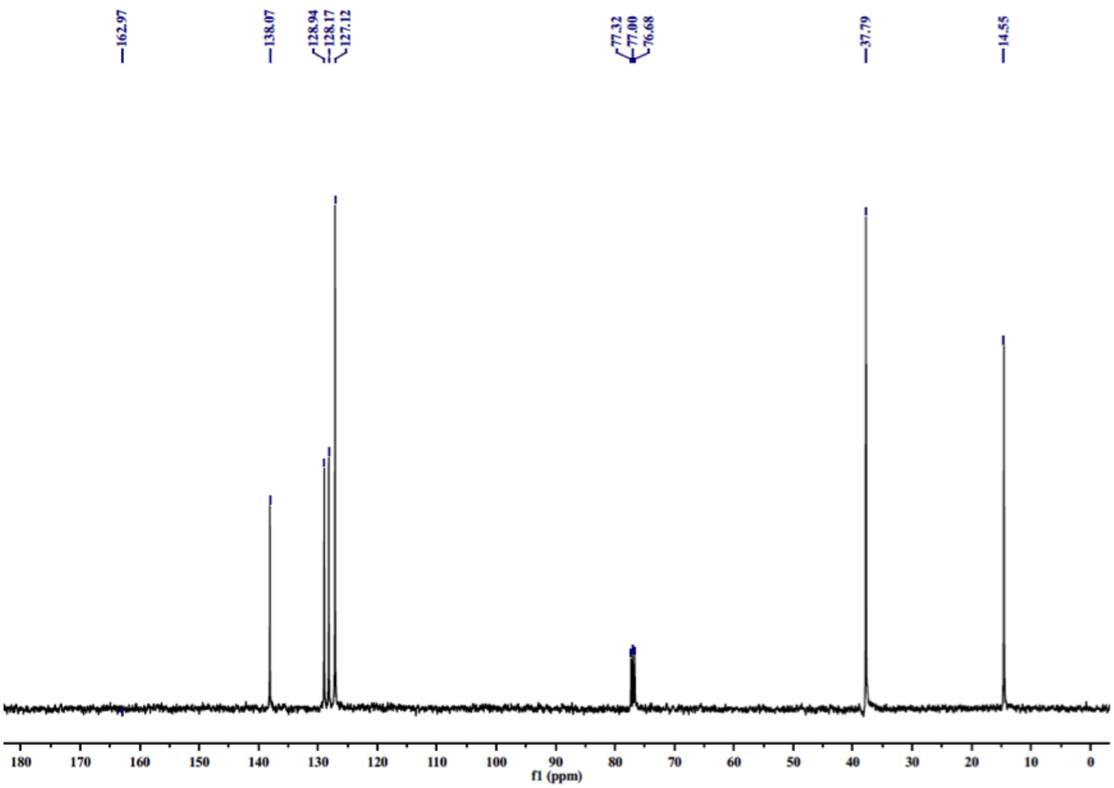

Figure S12: ^{13}C NMR spectrum of compound **2**.

conformations because the meta-linking of the benzene allows the closed benzene ”sandwich” to ”open”.[S6,S7] The surface area of the open conformer is larger than that of the closed. We therefore expect the equilibrium associated with open/closed conformer to be sensitive to the solvent. In the experiments we used a highly polar solvent (propylene carbonate) and we therefore expect the equilibrium to be shifted towards the closed conformer.

To confirm this, we calculated the relative free energy of the conformers with DFT using a range of functionals and incorporated the effect of solvent through the polarisable continuum model (PCM) using Gaussion09.[S8] We used the rather large 6-311++G(d,p) basis set. We used water as the solvent which has a dielectric constant similar to propylene carbonate (used in the experiment). We relaxed the geometries of the two conformers shown in Table 2 in both its ”open” and ”closed” form and evaluated the sum of the electronic and thermal free energy. The difference in the sum of electronic and thermal free energy of the two conformers ”open” and ”closed” form are shown in Table S1. Negative numbers indicate that the closed conformer has a lower energy. All functionals predict the closed structure to have the lowest energy. The energy difference ranged from 23.6-147.2 meV (k_BT is ≈ 25 meV at 25 ° C). DFT is likely to underestimate favorable long range interactions such as π-π-stacking which only occurs for the ”closed” conformer. PCM is likely to underestimate hydrophobic effects of the solvent on the ”open” structure due to larger surface area. Both effects are likely to decrease the free energy of the the closed conformer more than for open conformer. It is therefore probable, that the predominant conformer in the experiment are the closed conformers shown in Table 2 of the main paper.

Table S1: Free energy difference of open and closed structures (eV) (sum of electronic and thermal free energy). Negative numbers indicates that the closed conformer has lower free energy.

Conformer\Functional	PBE	B3LYP	CAM-B3LYP	M06-2X
meta-1	-0.1132	-0.1308	-0.1472	-0.0535
meta-2	-0.0246	-0.0541	-0.0516	-0.0230

References

(S1) Thygesen, K. S.; Rubio, A. *Phys. Rev. Lett.* **2009**, *102*, 1–4.

(S2) Borges, A.; Fung, E. D.; Ng, F.; Venkataraman, L.; Solomon, G. C. *J. Phys. Chem. Lett.* **2016**, *7*, 4825–4829.

(S3) Borges, A.; Solomon, G. C. *J. Chem. Phys.* **2016**, *144*, 194111.

(S4) Thygesen, K.; Hansen, L.; Jacobsen, K. *Phys. Rev. Lett.* **2005**, *94*, 26405.

(S5) Rasheed, O. K.; Bailey, P. D.; Lawrence, A.; Quayle, P.; Raftery, J. *European J. Org. Chem.* **2015**, *2015*, 6988–6993.

(S6) Annunziata, R.; Benaglia, M.; Cozzi, F.; Mazzanti, A. *Chem. - A Eur. J.* **2009**, *15*, 4373–4381.

(S7) Xia, J. L.; Liu, S. H.; Cozzi, F.; Mancinelli, M.; Mazzanti, A. *Chem. - A Eur. J.* **2012**, *18*, 3611–3620.

(S8) Frisch, M. J.; Trucks, G. W.; Schlegel, H. B.; Scuseria, G. E.; Robb, M. A.; Cheeseman, J. R.; Scalmani, G.; Barone, V.; Petersson, G. A.; Nakatsuji, H.; Li, X.; Caricato, M.; Marenich, A. V.; Bloino, J.; Janesko, B. G.; Gomperts, R.; Mennucci, B.; Hratchian, H. P.; Ortiz, J. V.; Izmaylov, A. F.; Sonnenberg, J. L.; Williams-Young, D.; Ding, F.; Lipparini, F.; Egidi, F.; Goings, J.; Peng, B.; Petrone, A.; Henderson, T.; Ranasinghe, D.; Zakrzewski, V. G.; Gao, J.; Rega, N.; Zheng, G.; Liang, W.; Hada, M.; Ehara, M.; Toyota, K.; Fukuda, R.; Hasegawa, J.; Ishida, M.; Nakajima, T.; Honda, Y.; Kitao, O.; Nakai, H.; Vreven, T.; Throssell, K.; Montgomery, J. A., Jr.; Peralta, J. E.; Ogliaro, F.; Bearpark, M. J.; Heyd, J. J.; Brothers, E. N.; Kudin, K. N.; Staroverov, V. N.; Keith, T. A.; Kobayashi, R.; Normand, J.; Raghavachari, K.; Rendell, A. P.; Burant, J. C.; Iyengar, S. S.; Tomasi, J.; Cossi, M.; Millam, J. M.; Klene, M.; Adamo, C.; Cammi, R.; Ochterski, J. W.; Martin, R. L.; Morokuma, K.; Farkas, O.; Foresman, J. B.; Fox, D. J. Gaussian16 Revision D.01. 2016; Gaussian Inc. Wallingford CT.